Geochemistry, Geophysics, Geosystems

RESEARCH ARTICLE
10.1029/2023GC011366

Morphology-Dependent Magnetic Properties in Shallow-Water Ferromanganese Concretions

Joonas Wasiljeff[1], Johanna M. Salminen[1,2], Andrew P. Roberts[3], Pengxiang Hu[3], Maxwell Brown[4], Jukka Kuva[1], Sari Lukkari[1], Ester M. Jolis[1], Atko Heinsalu[5], Wei-Li Hong[6,7], Aivo Lepland[5,8], Sten Suuroja[9], Joni Parkkonen[10], and Joonas J. Virtasalo[1]

[1]Geological Survey of Finland (GTK), Espoo, Finland, [2]Department of Geosciences and Geography, University of Helsinki, Helsinki, Finland, [3]Research School of Earth Sciences, Australian National University, Canberra, ACT, Australia, [4]Department of Earth and Environmental Sciences, Institute for Rock Magnetism, University of Minnesota, Minneapolis, MN, USA, [5]Department of Geology, Tallinn University of Technology, Tallinn, Estonia, [6]Department of Geological Sciences, Stockholm University, Stockholm, Sweden, [7]Baltic Sea Centre, Stockholm University, Stockholm, Sweden, [8]Geological Survey of Norway, Trondheim, Norway, [9]Geological Survey of Estonia, Rakvere, Estonia, [10]Department of Physics and Nanoscience Center, University of Jyväskylä, Jyväskylä, Finland

Key Points:

- Magnetic minerals within shallow water Fe-Mn concretions can provide valuable environmental information about their formation
- Magnetic properties are linked to specific growth patterns in Baltic Sea Fe-Mn concretions
- Spheroidal and crust/discoidal concretions are dominated by biogenic and pedogenic magnetic phases, respectively

Supporting Information:

Supporting Information may be found in the online version of this article.

Correspondence to:

J. Wasiljeff,
joonas.wasiljeff@gtk.fi

Citation:

Wasiljeff, J., Salminen, J. M., Roberts, A. P., Hu, P., Brown, M., Kuva, J., et al. (2024). Morphology-dependent magnetic properties in shallow-water ferromanganese concretions. *Geochemistry, Geophysics, Geosystems*, *25*, e2023GC011366. https://doi.org/10.1029/2023GC011366

Received 21 NOV 2023
Accepted 6 MAY 2024

Abstract Ferromanganese concretions commonly occur in shallow-water coastal regions worldwide. In the Baltic Sea, they can record information about past and present underwater environments and could be a potential source for critical raw materials. We report on their microstructural characteristics and magnetic properties and link them to their formation mechanisms and environmental significance. Microstructural investigations from nano- and micro-computed tomography, electron microscopy, and micro-X-ray fluorescence elemental mapping reveal diverse growth patterns within concretions of different morphologies. Alternating Fe- and Mn-rich growth bands indicate fluctuating redox conditions during formation. Bullet-shaped magnetofossils, produced by magnetotactic bacteria, are present, which suggests the influence of bacterial activity on concretion formation. Spheroidal concretions, which occur in deeper and more tranquil environments, have enhanced microbial biomineralization and magnetofossil preservation. Conversely, crusts and discoidal concretions from shallower and more energetic environments contain fewer magnetofossils and have a greater detrital content. Our results provide insights into concretion formation mechanisms and highlight the importance of diagenetic processes, oxygen availability, and bacterial activity in the Baltic Sea.

1. Introduction

Ferromanganese (Fe-Mn) concretions are distributed widely, extending beyond deep ocean environments to encompass the shelf seas of the world, with notable occurrences in the north-eastern Atlantic Ocean, South China Sea, Kara Sea, Black Sea, Barents Sea, and Baltic Sea (Baturin, 2010; González et al., 2010; Vereshchagin et al., 2019; Zhamoida et al., 2017; Zhong et al., 2017). In the Baltic Sea, early reports of Fe-Mn concretions were made in the late 19th and early 20th centuries (e.g., Grewingk, 1884; Hessle, 1924), but the first major studies of these precipitates were not carried out until the 1960s and 1970s (e.g., Glasby et al., 1997; Winterhalter & Siivola, 1967). Recently, Fe-Mn concretions have gained increased economic and scientific attention globally due to their importance as underwater habitats, as sources of critical metals, and due to their ability to record paleoceanographic and paleoenvironmental changes (e.g., Hannington et al., 2017; Hein et al., 2020; Jiang et al., 2022; Kaikkonen et al., 2019).

Authigenic Fe-Mn concretion formation is typically confined to the seafloor in areas experiencing low or no net sediment deposition and organic matter loading with colloidal iron and manganese oxyhydroxides supplied from the surrounding catchment area and/or from adjacent anoxic marine sediments due to diagenetic remobilization (Ingri & Pontér, 1986; Marcus et al., 2004; Zhamoida et al., 2007). Their formation is redox driven and often creates concretions with alternating Fe and Mn layers reflecting redox fluctuations (Axelsson et al., 2002; Gasparatos et al., 2005; Winterhalter & Siivola, 1967). Fe and Mn (oxyhydr)oxides effectively scavenge trace elements, including cobalt and rare earth elements (REEs), from seawater, which attests to their economic importance. Typically, the Fe and Mn phases are poorly crystalline or X-ray amorphous Fe and Mn hydroxides, but 2-line ferrihydrite and turbostratic birnessite have also been observed (Marcus et al., 2004). In the Baltic Sea, concretions are porous and have various sizes and shapes (i.e., crust, discoidal, and spheroidal) and harbor diverse microbial communities with reductive and oxidative metabolisms that can influence both concretion growth and

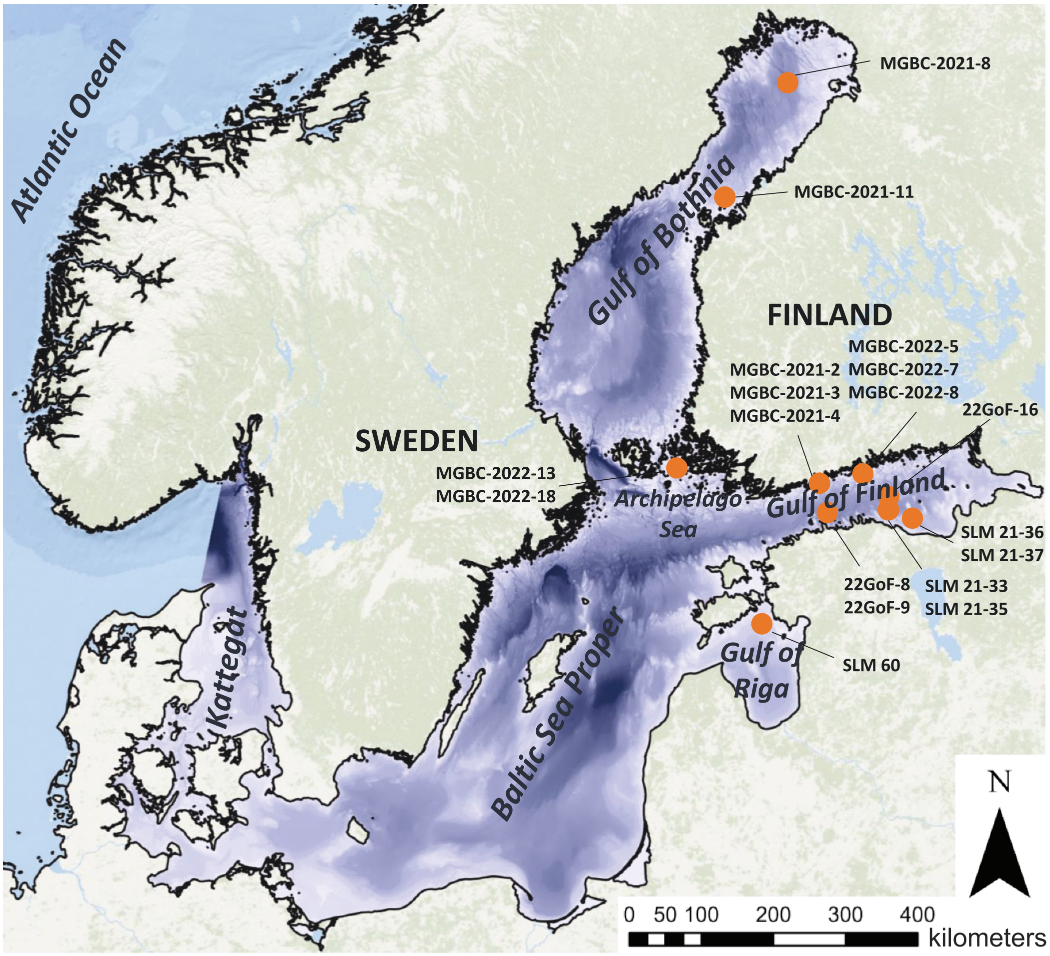

Figure 1. Map of Fe-Mn concretion sample locations (orange circles) in the Baltic Sea region. Bathymetry is presented only for the Baltic Sea basin. Base map: ESRI Inc. (Redlands) Ocean Basemap 2018. Bathymetric data: EMODnet Bathymetry 2018 (Thierry et al., 2019).

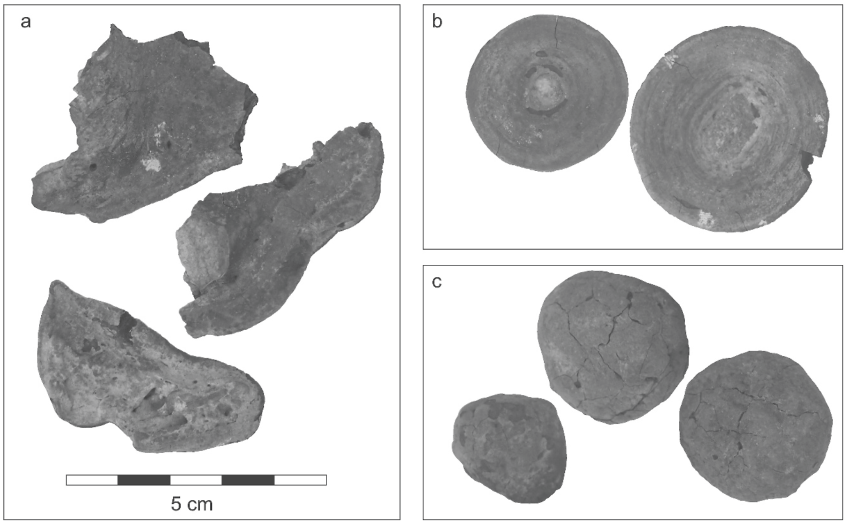

Figure 2. End member morphotypes of Baltic Sea Fe-Mn concretions. (a) Crust, (b) discoidal, and (c) spheroidal. All images have the same scale. Irregular concretions and unique combinations of the three types are also common.

10.1029/2023GC011366

Table 1
List of Studied Fe-Mn Concretion Samples From the Baltic Sea

Sample name	Morphotype	Location	Latitude (N)	Longitude (E)	Water depth (m)
MGBC-2021-2-S-T1	Spheroidal	GoF	59°57.591	24°46.101	57.2
MGBC-2021-2-S-T2	Spheroidal	GoF	59°57.591	24°46.101	57.2
MGBC-2021-2-S-T3	Spheroidal	GoF	59°57.591	24°46.101	57.2
MGBC-2021-2-S-T4	Spheroidal	GoF	59°57.591	24°46.101	57.2
MGBC-2021-3-S-T1	Spheroidal	GoF	59°57.846	24°46.440	50.9
MGBC-2021-3-S-T2	Spheroidal	GoF	59°57.846	24°46.440	50.9
MGBC-2021-3-S-T3	Spheroidal	GoF	59°57.846	24°46.440	50.9
MGBC-2021-8-S-T1	Spheroidal	GoB	64°52.027	23°14.624	73.0
MGBC-2021-8-S-T2	Spheroidal	GoB	64°52.027	23°14.624	73.0
MGBC-2021-8-S-T3	Spheroidal	GoB	64°52.027	23°14.624	73.0
MGBC-2021-8-S-T4	Spheroidal	GoB	64°52.027	23°14.624	73.0
MGBC-2021-8-S-T5	Spheroidal	GoB	64°52.027	23°14.624	73.0
MGBC-2021-8-S-T6	Spheroidal	GoB	64°52.027	23°14.624	73.0
MGBC-2022-8-D/S-T1	Spheroidal	GoF	60°01.000	26°04.812	60.0
SLM 21-33-S-T1	Spheroidal	GoF	59°40.470	26°33.120	30.8
MGBC-2022-7-S-T1	Spheroidal	GoF	60°05.493	25°57.789	44.0
MGBC-2022-7-S-T2	Spheroidal	GoF	60°05.493	25°57.789	44.0
MGBC-2022-7-4	Spheroidal	GoF	60°05.493	25°57.789	44.0
MGBC-2022-7-fluffy	*Organic-rich mud*	GoF	60°05.493	25°57.789	44.0
22GoF-8_LAB1	Spheroidal	GoF	59°43.510	24°53.570	95.0
22GoF-9_LAB1	Spheroidal	GoF	59°43.534	24°53.662	95.0
22GoF-16-1	Spheroidal	GoF	59°55.110	26°20.537	80.0
MGBC-2021-4-1	Crust	GoF	59°57.929	24°46.726	45.4
MGBC-2021-4-C-T1	Crust	GoF	59°57.929	24°46.726	45.4
MGBC-2021-4-C-T2	Crust	GoF	59°57.929	24°46.726	45.4
MGBC-2021-4-C-T3	Crust	GoF	59°57.929	24°46.726	45.4
MGBC-2021-11-C-T1	Crust	GoB	63°33.747	21°54.616	32.2
MGBC-2021-11-C-T2	Crust	GoB	63°33.747	21°54.616	32.2
MGBC-2021-11-C-T3	Crust	GoB	63°33.747	21°54.616	32.2
MGBC-2022-13-C-T1	Crust	AS	60°05.569	21°16.312	51.0
MGBC-2022-13-C-T2	Crust	AS	60°05.569	21°16.312	51.0
SLM 60-D-T1	Discoidal	GoR	58°9.670	23°30.369	27.0
SLM 21-35-D-T1	Discoidal	GoF	59°38.673	26°43.073	36.2
SLM 21-37-D-T1	Discoidal	GoF	59°33.000	26°52.272	30.8
SLM 21-36-D-T1	Discoidal	GoF	59°33.034	26°52.259	31.2
MGBC-2022-5-D-1	Discoidal	GoF	60°11.483	26°01.895	29.0
MGBC-2022-18-D-T1	Discoidal	AS	60°02.746	21°35.102	18.0

Note. Abbreviations for locations in the Baltic Sea: AS = Archipelago Sea, GoB = Gulf of Bothnia, GoF = Gulf of Finland, GoR = Gulf of Riga. Samples with the prefix SLM are provided by the Tallinn University of Technology, Estonia.

Geological Survey of Finland (GTK), Espoo, Finland. After drying, the samples became fragile and were impregnated with epoxy resin (Struers EpoFix). The resin-embedded concretions were then cut in half. One other half was prepared into an epoxy button or thin section for electron microscope imaging and micro-X-ray fluorescence (µXRF) analyses at the GTK and the other half was cut into slices perpendicular to growth layers with a

. 8 0' 7 3 7) 7 . ,
, . (C 8 7
-7 .
8

0 . M (
M (8M . 7 (S . 33 %F
2/- 7 (S , - - . % ' 7 % (8
(S . S S PS 8%
% . 33 (, 3 N .
% ' M %7 %8 % . .
4 3 4 8% . . %
. . 8 7
S% FS S% FS S% F 33 (S F 33 % 33 E
. 8S% FS S% F 33 (; (
33) 3 B 8 3 8 33 33 8
T U % 33 V % 33 F 33OW
. % 33 (.
0 33 8

S 8 . .
. % ' MK7 7 (8 . / 33Q
(. ((. 8
' 1S8 8 . JFE . . 8 8 . ' 8

7 ' .
% & %& ' (% . 4 '
233 (A
% M 1-33 A 8 ('
4 8 222 (8 333 .
8 3 1 (8 3 2 B 8 3 / B 8 3 /
. . ' ' '
8

. . ; ') 8S . B 8 3 , (E
J . (. 33 , 33 8
. ' 7 . ; '
. 8% 33 . . . 8
. (7 . 7 - 7 0' 7
3 7) 7 8 . , 33 .
33 8 ' .
8 . , 3 (8 8% / 33 N
. / ' 8 8 3 '
8 33 8 ' . ' . D (331
A% ' 3 8' . ('
;
. %: ; . ; (8 3 - 8

M . 7 (. . X
4 4 7 . 4 : M/ %& 8
. . 3 33 33 3
8 , %& ' B ' . 8 , 3
8 . . 7 33
7 . . 8 , .
33 . . . 33 3 . 33 8

Table 2
Magnetic Properties of Baltic Sea Fe-Mn Concretions

Sample name	χlf (10^{-8} m^3 kg^{-1})	χfd (10^{-8} m^3 kg^{-1})	χARM (10^{-8} m^3 kg^{-1})	IRM_{100} (10^{-5} Am^2 kg^{-1})	SIRM (10^{-5} Am^2 kg^{-1})	$HIRM_{AF100}$ (%)	χARM/ χlf (−)	χARM/ χfd (−)	χARM/IRM_{100} (10^{-3} mA^{-1})	χlf/IRM_{100} (mA^{-1})
MGBC-2021-2-S-T1	34	1.2	226	163	175	6.8	6.8	196	1.4	205
MGBC-2021-2-S-T2	32	1.2	185	137	148	7.1	5.8	151	1.3	231
MGBC-2021-2-S-T3	37	-	200	144	156	7.4	5.4	-	1.4	257
MGBC-2021-2-S-T4	32	0.4	183	137	147	7.0	5.7	445	1.3	236
MGBC-2021-3-S-T1	45	0.8	242	182	201	9.5	5.3	309	1.3	249
MGBC-2021-3-S-T2	41	1.0	215	162	179	9.6	5.3	221	1.3	252
MGBC-2021-3-S-T3	46	0.6	242	179	200	10.3	5.3	376	1.4	254
MGBC-2021-8-S-T1	78	1.8	457	807	863	6.4	5.8	260	0.6	97
MGBC-2021-8-S-T2	78	1.9	430	753	802	6.1	5.5	223	0.6	103
MGBC-2021-8-S-T3	79	1.5	385	766	819	6.4	4.9	254	0.5	103
MGBC-2021-8-S-T4	75	1.4	420	741	791	6.4	5.6	304	0.6	102
MGBC-2021-8-S-T5	82	1.1	370	714	764	6.6	4.5	331	0.5	115
MGBC-2021-8-S-T6	104	0.5	311	719	774	7.1	3.0	692	0.4	144
MGBC-2022-8-D/S-T1	42	0.7	231	-	-	-	5.5	333	-	-
SLM 21-33-S-T1	39	0.4	117	91	101	10.3	3.0	316	1.3	430
MGBC-2022-7-S-T1	45	0.6	178	120	134	10.2	3.9	286	1.5	375
MGBC-2022-7-S-T2	43	0.6	302	-	-	-	7.1	487	-	-
22GOF-8_LAB1	51	1.0	470	175	180	2.8	9.2	453	2.7	293
22GOF-9_LAB1	45	1.0	234	-	-	-	5.3	235	-	-
22GoF-16-1	-	-	194	83	88	5.5	-	-	2.3	-
Spheroidal mean	54	1.0	280	357	384	7.4	5.4	326	1.2	215
SD	21	0.5	106	301	321	2.0	1.4	129	0.6	100
MGBC-2021-4-C-T1	32	0.5	36	34	67	49.1	1.1	69	1.1	930
MGBC-2021-4-C-T2	31	0.4	18	19	58	66.8	0.6	52	1.0	1,600
MGBC-2021-4-C-T3	27	0.5	14	16	60	72.8	0.5	29	0.9	1,644

Table 2
Continued

Sample name	χlf (10^{-8} m^3 kg^{-1})	χfd (10^{-8} m^3 kg^{-1})	χARM (10^{-8} m^3 kg^{-1})	IRM_{100} (10^{-5} Am^2 kg^{-1})	SIRM (10^{-5} Am^2 kg^{-1})	$HIRM_{AF100}$ (%)	χARM/ χlf (−)	χARM/ χfd (−)	χARM/IRM_{100} (10^{-3} mA^{-1})	χlf/IRM_{100} (mA^{-1})
MGBC-2021-11-C-T1	50	1.1	107	520	586	11.3	2.1	98	0.2	95
MGBC-2021-11-C-T2	54	3.2	211	-	-	-	3.9	66	-	-
MGBC-2022-13-C-T1	34	0.5	70	38	51	25.4	2.0	144	1.8	896
MGBC-2022-13-C-T2	39	0.4	191	-	-	-	4.9	469	-	-
Crust mean	38	0.9	92	126	165	45	2.2	132	1.0	1,033
SD	10	1.0	81	221	236	26	1.7	153	0.6	633
SLM 60-D-T1	40	0.3	79	47	76	37.6	2.0	263	1.7	840
SLM 21-35-D-T1	36	0.2	117	81	93	13.7	3.2	472	1.5	449
SLM 21-37-D-T1	42	0.5	118	82	97	15.3	2.8	221	1.4	506
SLM 21-36-D-T1	39	0.3	118	86	100	13.7	3.0	347	1.4	451
MGBC-2022-18-D-T1	28	0.4	45	37	52	28.1	1.6	115	1.2	741
Discoidal mean	37	0.4	96	67	84	22	2.5	284	1.4	598
SD	5	0.1	33	23	20	11	0.7	134	0.2	181
MGBC-2022-7-fluffy	20	0.3	133	83	106	21.7	6.5	381	1.6	246
Total mean	47	0.9	208	255	287	17	4.3	277	1.2	437
SD	19	0.6	128	279	298	19	2.0	152	0.6	422

slightly lower as indicated by lower χARM (Table 2). This discrepancy could result from the slower growth of deep ocean Fe-Mn precipitates and an increased terrigenous influence on Baltic Sea concretions, which is attributed to their contrasting marine settings.

Low values of HIRM for spheroidal concretions suggest they are devoid of magnetically hard minerals ($B_{cr} > 100$ mT, such as hematite or goethite), whereas harder minerals (greater HIRM values) are present in crust and discoidal concretions (Figure 3a). Thermomagnetic analyses indicate that in spheroidal samples, subtle susceptibility increases start from ∼270°C with a peak at ∼300°C. A large increase occurs at ∼400°C peaking at ∼500°C in all morphotypes, followed by a drop across the Curie temperature of magnetite (Figures 4a–4c). These changes in susceptibility may be caused by the conversion of paramagnetic phases into stable Fe phase minerals. Cooling curves are irreversible and indicate the formation of new magnetic materials during heating.

In low-temperature, most of the measured samples display a marked drop in remanence between ca. 10 and 50 K in the FC and ZFC curves (Figures 4d–4p; Figures S3 and S4 in Supporting Information S1). Inflections at around 20 K and sometimes at 35 K could suggest the presence of rhodochrosite with differing Fe and Mn contents and impurities (Frederichs et al., 2003). Rhodochrosite is the most prominent in the spheroidal sample 22GoF-16-1 data (Figure 4g and Figure S3 in Supporting Information S1), which is consistent with the phase having peaks in low-temperature susceptibility in both the in-phase and out of phase components at around 35 K (Figure 4d; Kosterov et al., 2006). Additional evidence for the presence of rhodochrosite is provided by hysteresis loops measured at 25 and 35 K (Figure S5 in Supporting Information S1), revealing a distinct ferrimagnetic component, while at 50 K, the loop predominantly exhibits paramagnetic characteristics (see Kars et al., 2011; Kosterov et al., 2006).

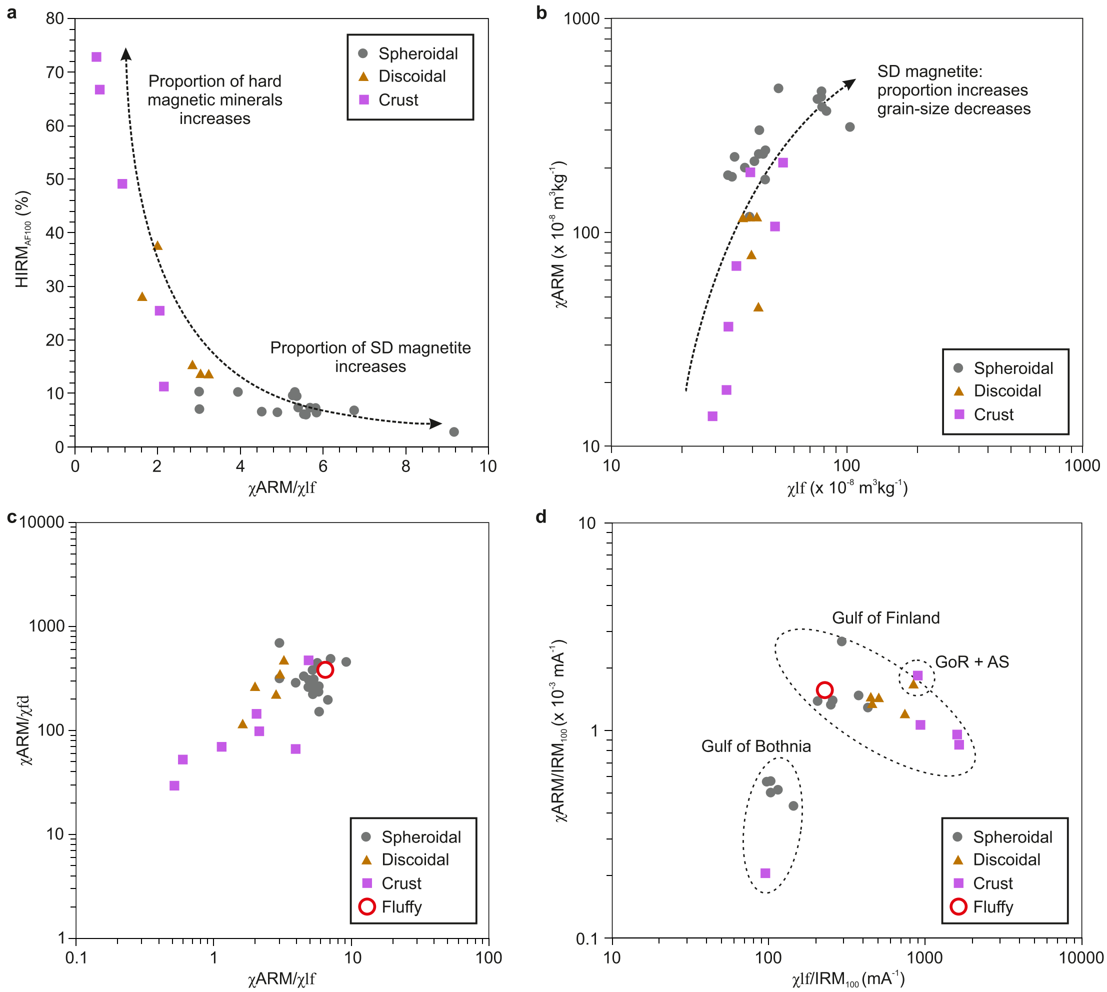

0 7 8 % 33 S% FS .
(. 33 % 33 7 S% FS 8 (S%
S 0 C 8 21 8 21 . (8 0 7 S% FS
S% FS ((7 3 8 0 S% F
33 S F 33 8% % 8

' 7B ' 7) P) 8
. . (A . E
33 3) . . ; (
' 8 3 - 5 D . 3 8 E
(.
. ' B ')
)) 8 (;
. (
212 M 8 33- D 212 8 3 D 3 3 8
7 . . (33
3)) C)
; D 3 3 8
S% S
. (8
S (
4 7 (8' '

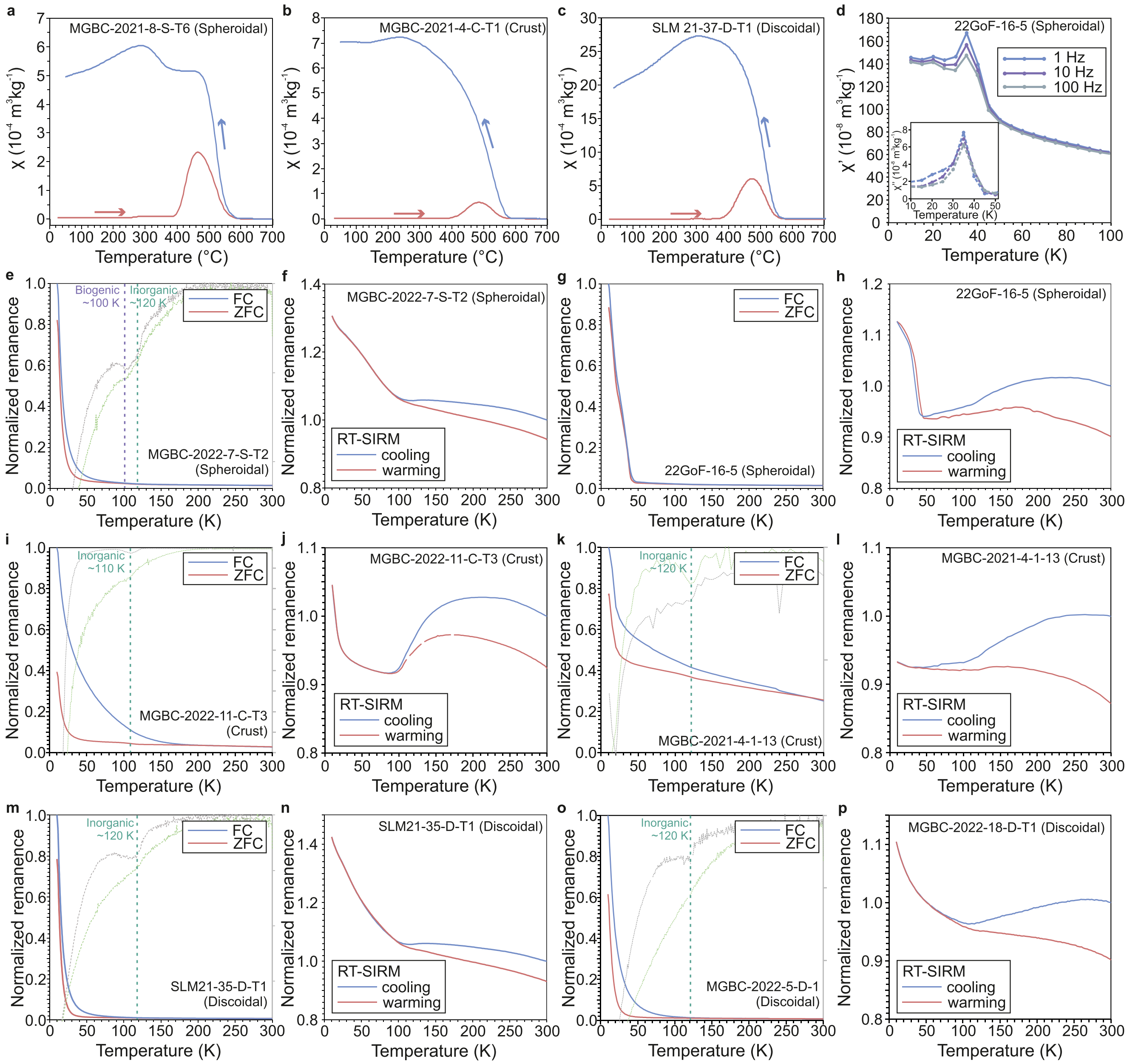

0 7 8 P S (
8 M . 7 7 7 %' (7 - 7 7, 8 ' B '
8& ' B ' 8 C
7 . 8

. (; , 1
8 (8 3 2 8% ' / E
47 (
8 3 2 B 8 3 / 7 ;
. (8 3 3 8 3) 8 (7
S% FS S% FS . 7 8 .
; .
(. . (7
(8 (. 8

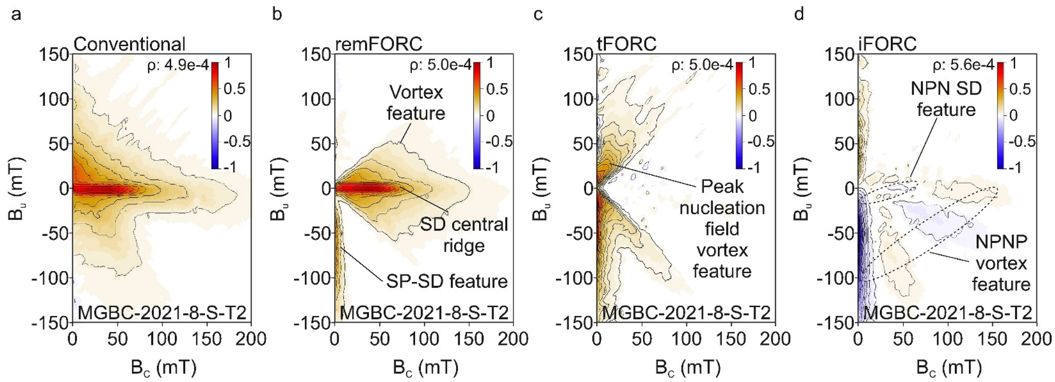

7 ' 4 8 222 (8 333
0' 7 3 7/7 7 0 0 0 8
' ' . ; ((8 (8 3 2 8
(' ('
; . ; (4F
4 8 33 B 8 3 / 8 % ' . ;
((8 3 / B 8 3 / 8 ' .
7 7 &4& ; (7 7 7 &4&4 B
8 3 / 8

S% F 33 S F 33 ((0
. % 8
(. (; S% F 33 (; S F
33 (. (
8 ; . ((
8 (7 0' 7
3 7/7 8

(7 (.
; (4 ; 7 7 .
; . ((- 8

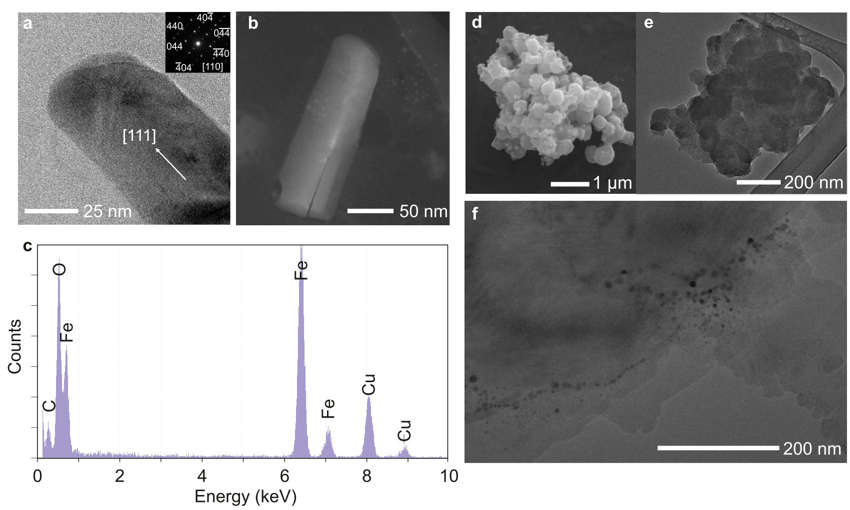

0 (7 0 7 8 7
. . ((
8 8' ' (8 7
7 ; ; . 8 0 7
; 8 0 7 ; (47 8

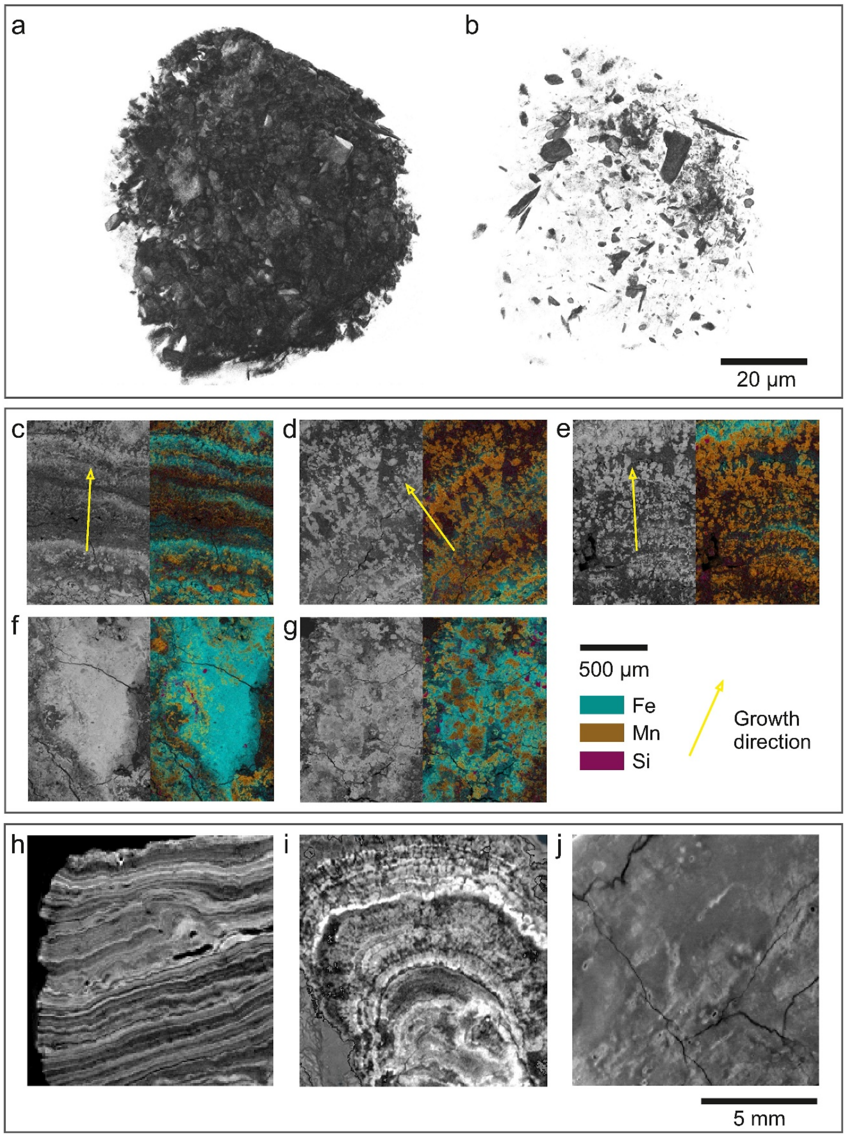

1 0 7 J & ' 7 ;
(; (8 P 7 0
PC N 8' J P
C 8 . (. . 8

. . 7 % 7 7
2(3 8

. .
2 2 - /
8' ; (7
((; (. J . . J 1P /
4J 38 , P38 3 38 . . J)) P2
- 4J 38 / P38 / 38 J , P/ , - 2 4J
38 2P38 - 38 2 2 8 .
33 M D 4 3 ; (8 3 - 8 3 .
. (0 (0
((33) 33) (33) 8 0 .

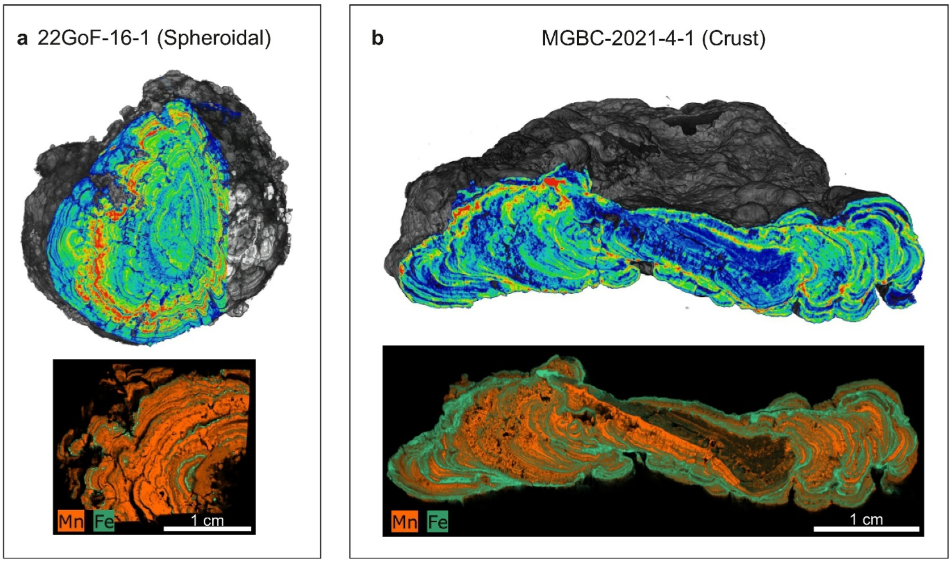
a 22GoF-16-1 (Spheroidal)
Mn
Fe
1 cm
b
MGBC-2021-4-1 (Crust)
Mn
Fe
1 cm

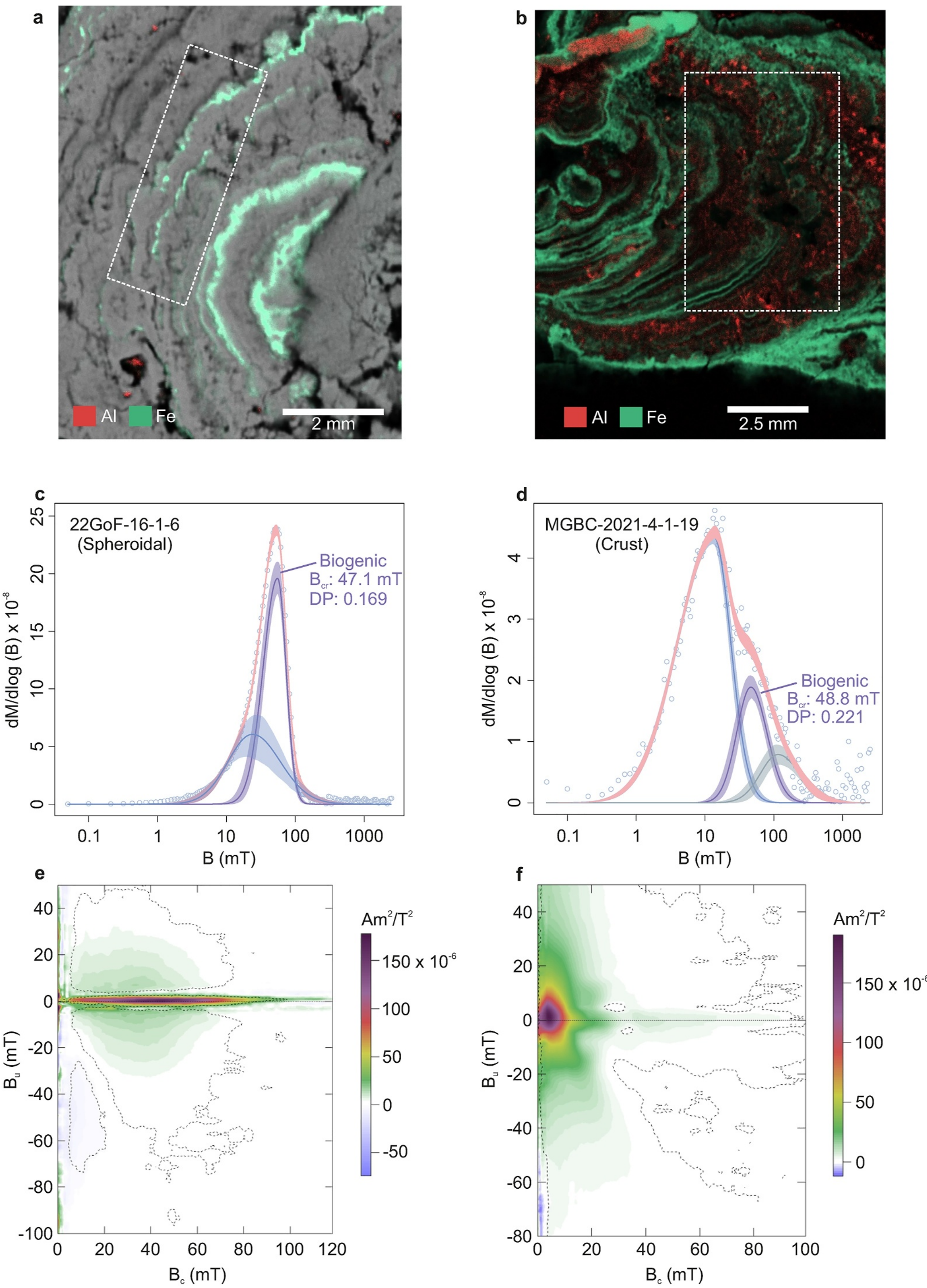

3 ' 7 - 7 0' 7 3 7)7 8 (N % 89 (; ; . . P 8 ' ; . (. (. (8 ' ' 8 (7 . 8

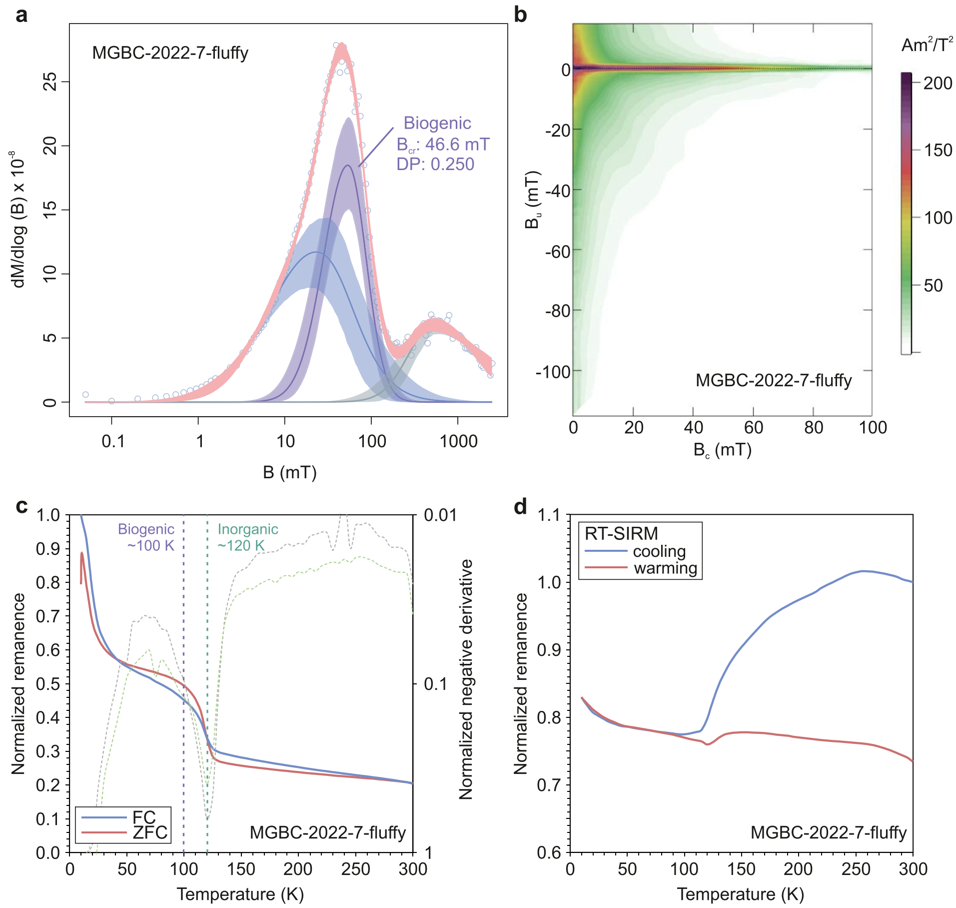

a
MGBC-2022-7-fluffy
Biogenic
B_cr: 46.6 mT
DP: 0.250
dM/dlog (B) x 10^-8
B (mT)
b
Am²/T²
MGBC-2022-7-fluffy
B_u (mT)
B_c (mT)
c
Biogenic
~100 K
Inorganic
~120 K
FC
ZFC
MGBC-2022-7-fluffy
Normalized remanence
Normalized negative derivative
Temperature (K)
d
RT-SIRM
cooling
warming
MGBC-2022-7-fluffy
Normalized remanence
Temperature (K)

ADVANCING EARTH AND SPACE SCIENCES

(%848 48 858 8 ;. %8 8 8 8 3 2 8 J 8 3 - , 1- P,) 8 JIF 8 F 38 3 2F 3 1503 / 3) 2
(%848 4 ' 8 8 D A (8M8 333 8 7 J% . 8 0 1) - P 1) / , 8 JIF 8 F 38 3 2F 33350 233 -
48 D 8 212 8 (J4 8 2 1 1, P1,) 8 JIF 8 F 38 3 2F M8 - 331 331,
8 5 M8 8 8 8' 8 0 8 8 3 2 8 (@ c 0 8 3 P 38 JIF 8 F 38 3 2F 3 1503 -, / -
8 5 M8 (%8 8' 58 %(8 D M 8 3 1 8 ; ((8 6 - / P) 8 JIF 8 F 38 F / , 17 28 -))
&8 %(8 %8 8 D 8 3 8 7 . % P 8 2- / 8 JIF 8 F 38 3 1F) , 2173 7)) 27-
58 589 8 . 8 8 D 0 8 3 8 . J% 8 4 (. . ; 8 8 JIF 8 F 38 12F 8 3 8 3) 3
8 8 8 0 M8 D ' 48 3 2 8 0 (. 8 1 : 1 8 P/ 8 JIF 8 F 38 32F ' %& 8 3 28 1- / , 3
K8 K 8 D 8 3 / 8' (
9 & 4 8)), , 1P), / 8 JIF 8 F 38 33 F 3 / ' 33/ /
A 8 8 4 8&8 0 %8 8 A80 8 %8 8 A8A8 D 8A8 3 2 8 7 J 8 6 5 2 2 P 3) 8 JIF 8 F 38 3 - K8 8 3 28 88
A 5858 D %8 8 331 84 (7. % 0 8 P P 8 JIF 8 F 38 3 - K8 8 33 18 8 831
9 ' 8M8 M 8 M 48' 8 8 M 858 8 D 80 8 3 8 7(4 7 ; J ; 8 (2 , 3 4%33) , 8 JIF 8 F 38 3 2F 3 4%33) ,
9 C 58 D 58 3 8 % . V W8 6 : 8 JIF 8 F 38 / 2F 2 / / 1 722 / 17) 1 71 7 3 (3 (3
9 C 58 58 8 (%848 48 0 . 8 58 8 3) 8 7 . 7 . V W8 8 JIF 8 F 38' 11FA) F % ' F 332/
9 0 8 213 8 0 8 8 8A D 8 8 8 / P ,) 8 % 8
9 0 8 D 58 2- / 8% ((0 0 8 7 - P / 8
K 8 9 8 8 D K8 3 3 8 ; (4 7 8 & 38 JIF 8 F 38 1- F) 3- 73 373) 17,
K 8 D . 8 221 8 (; 8 2 3-) P 3- - 8 JIF 8 F 38 3F 332 7/ - 221 3 - 3-) J 8 8
K 7 48 5e 8 8 D M 58 3) 8 P (0 J (7 ; 8 - ( ) - P / , 8 JIF 8 F 38 313F 3) 23), 8 3 8 23, 3
K 8 D M (58 8 3 3 80 ; 8)(/ 1 -), P), 18 JIF 8 F 38 3 1F) , 1- 73 37) - 17,
K 9 8 B 8 K B8 58 8 D K X8 3 3 8 (8 3) 21P 3 8 JIF 8 F 38 3F) - 11 8
B A8 %8 8 D (8 33/ 8 7 8 6 3 P 8
B A8 %8 (8 %8 %8 8 A 8 D %8 8 3 / 8 E Y (8 & / 1P 1/ 8 JIF 8 F 38 3 - K8C 8 3 / 8 8 8 32
B A8 %8 0 9 848 (848 D 4 8 %8 22- 8 0 8 3 - P / - 8 JIF 8 F 38 313F 3-) 22- 32 11 32
B 8 8 M ' 8K8 0 M8B8 (848 D B A8 33 84 ((E 0 8 P 28
B X8 (%848 8 M K8 M 58 M 8 8 3 8 7 8 & 3 503)) 8 JIF 8 F 38 3 2F 3 503))
B : 8 8 D (%848 3 , 8% (7 7 8 2 , -) P / / 8 JIF 8 F 38 33 F 3) ' 33, - 13
B : 8 (%848 8 4 8%8 M K8 D M 58 3 / 8 8 /) / - / P) / 128 JIF 8 F 38 33 F 3 - 503 - 1
B K8 ' B8 @ 858 58 8 B : 8 M 8 8 3 / 8' ' 8 1 () 3P 18 JIF 8 F 38 3 - K8C 8 3 / 8 8 8 ,